Journal of Solid State Chemistry 186 (2012) 81–86

Contents lists available at SciVerse ScienceDirect

Journal of Solid State Chemistry

journal homepage: www.elsevier.com/locate/jssc

Electronic structure and chemical bonding of α- and β-$CeIr_2Si_2$ intermediate valence compounds

Samir F. Matar [a,*], Rainer Pöttgen [b], Bernard Chevalier [a]

[a] CNRS, Université de Bordeaux, ICMCB, 87 Avenue du Docteur Albert Schweitzer, 33600 Pessac, France
[b] Institut für Anorganische Universität Münster, Corrensstrasse 30, D-48149 Münster, Germany

ARTICLE INFO

Article history:
Received 19 September 2011
Received in revised form
21 November 2011
Accepted 26 November 2011
Available online 4 December 2011

Keywords:
Intermetallic compounds
$CeIr_2Si_2$
Electronic structure
Equation of state
Dimorphism

ABSTRACT

The dimorphism of the intermediate valence ternary cerium silicide $CeIr_2Si_2$ in the $ThCr_2Si_2$ (α) and $CaBe_2Ge_2$ (β) modifications is addressed in the framework of the density functional theory. The geometry optimization is in good agreement with the experiment and the subsequent establishment of the energy–volume equation of state (EOS) indicates a stabilization of the β-type relative to the α-type concomitant with the trend of the cerium valence, changing to tetravalent in β-$CeIr_2Si_2$. This is equally shown from the site projected DOS and from the large increase of the electronic contribution to the specific heat. The chemical bonding indicates the strongest bonding interactions within the Ir–Si substructure in both varieties. Stabilization of β-$CeIr_2Si_2$ with almost tetravalent cerium is in good agreement with $Th^{IV}Ir_2Si_2$ which exclusively crystallizes in the $CaBe_2Ge_2$ type. The EOS behavior of different RIr_2Si_2 (R=Th, Ce, La) is comparatively discussed.

1. Introduction

Among the huge number of rare earth (*Ln*)-based intermetallic compounds, those with structures that are derived from the tetragonal $BaAl_4$ type [1] comprise one of the largest families [2,3]. These phases have intensively been studied in the last 40 years by solid state chemists and physicists with respect to their broadly varying physical properties [4] and this research topic recently gained a true renaissance, when superconductivity at T_{max}=38 K was observed for the solid solution $Ba_{1-x}K_xFe_2As_2$ [5,6].

The two simplest ternary substitution variants of the $BaAl_4$ structure are the $ThCr_2Si_2$ [7] and $CaBe_2Ge_2$ [8] types, where the chromium and silicon, respectively, beryllium and germanium atoms are ordered in two different manners on the aluminum substructure (Fig. 1). Besides these two structure types with almost 1000 representatives [3], diverse other substitution and distortion variants have been reported [9,10], which derive from the aristotype $BaAl_4$ via group–subgroup relations.

A very interesting phenomenon in the series $LnIr_2Si_2$ and $LnNi_2As_2$ is the occurrence of temperature driven dimorphism with a $ThCr_2Si_2$ type low- and $CaBe_2Ge_2$ type high-temperature modification [11]. Since the phase transition is of a reconstructive type, both modifications can be characterized under ambient conditions. This is especially interesting for cerium, europium, and ytterbium containing compounds, since for these materials valence changes and drastic differences in the physical properties can be expected.

Such temperature driven dimorphism occurs for the ternary silicide $CeIr_2Si_2$ [11]. β-$CeIr_2Si_2$ crystallizes directly from the melt, while α-$CeIr_2Si_2$ forms after annealing at 870 K [12,13]. The modifications of this compound have intensively been studied with respect to the magnetic and electrical properties [12,14–20]. Thermal expansion measurements show large hysteresis for the phase transition [20]. Temperature dependent magnetic susceptibility measurements and cerium XL_{III} absorption edges at 300 K [12,18] show that both modifications remain paramagnetic down to low temperature and reveal intermediate cerium valence. At room temperature α-$CeIr_2Si_2$ has a cerium valence of 3.32, while β-$CeIr_2Si_2$ tends towards tetravalent cerium with a value of 3.56 [12]. The intermediate cerium valence expresses itself in the course of the cell volumes in the $LnIr_2Si_2$ series. The $CeIr_2Si_2$ cell volumes are close or even smaller than those of $PrIr_2Si_2$. Also the intermediate cerium valence seems to weaken the overall chemical bonding. This is nicely reflected in the course of the phase transition temperatures which is the lowest one for the cerium compound in the series $LnIr_2Si_2$ (Ln=La, Ce, Pr, Nd) [20].

On the theoretical side, several works were devoted to the calculated electronic structure of intermetallic compounds with 1:2:2 stoichiometry such as the early study of the bonding in $ThCr_2Si_2$ and $CaBe_2Ge_2$ type main group solids by Zheng [21], $SrPt_2As_2$ [22] and dimorphism effects in YIr_2Si_2 [23] and $LaIr_2Si_2$ [24].

* Corresponding author. Fax: +33 5 4000 27 61.
E-mail addresses: matar@icmcb-bordeaux.cnrs.fr (S.F. Matar), pottgen@uni-muenster.de (R. Pöttgen), chevalie@icmcb-bordeaux.cnrs.fr (B. Chevalier).

0022-4596/$ - see front matter © 2011 Elsevier Inc. All rights reserved.
doi:10.1016/j.jssc.2011.11.041

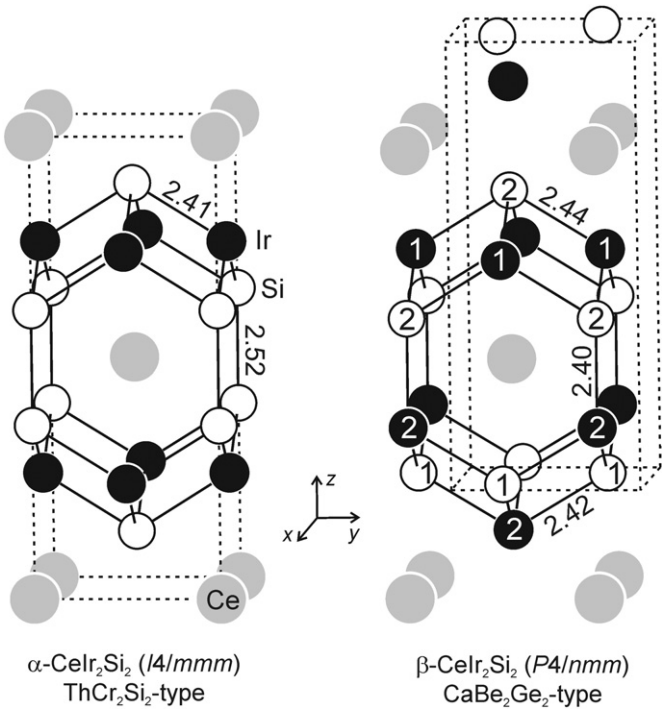

Fig. 1. The crystal structures of α- and β-$CeIr_2Si_2$. Relevant interatomic distances (Å), the three-dimensional $[Ir_2Si_2]$ networks and the crystallographically independent iridium and silicon sites are indicated.

Although both modifications of $CeIr_2Si_2$ have intensively been studied with respect to their magnetic, electrical and thermal expansion behavior, the electronic structure and chemical bonding have not been investigated. In the course of our systematic studies of chemical bonding in $Ce_xIr_yX_z$ intermetallics [25–29] we have now studied α- and β-$CeIr_2Si_2$ by *ab initio* electronic structure calculations within the well established quantum theory framework of the density functional theory (DFT) [30,31]. $CeIr_2Si_2$ is one of the rare intermetallic cerium compounds exhibiting a valence change that is accompanied by a switch in crystal structure, making it a model compound for the investigations of crystal structure–property and electronic structure–property relationships.

2. Crystal chemistry

The structures of α- and β-$CeIr_2Si_2$, as obtained from single crystal diffractometer data [13] are presented in Fig. 1. The cerium atoms in both modifications have coordination number 16 by 8 Ir+8 Si atoms. As emphasized in Fig. 1, due to the different coloring of iridium and silicon on the aluminum substructure of $BaAl_4$, the range in Ce–Ir and Ce–Si distances is different in both modifications. While the Ce–Si distances (8×3.155 Å in α-$CeIr_2Si_2$; 4×3.180 and 4×3.181 Å in β-$CeIr_2Si_2$) are almost similar, the Ce–Ir distances (8×3.262 Å in α-$CeIr_2Si_2$; 4×3.155 and 4×3.260 Å in β-$CeIr_2Si_2$) are distinctly different. The shorter Ce–Ir distances in β-$CeIr_2Si_2$ are a consequence of the almost tetravalent character of cerium, strengthening the Ce–Ir bonding. Such behavior has repeatedly been observed in diverse $Ce_xRu_yX_z$ (X=Mg, Cd, Al, In, Sn) intermetallics [32,33] with intermediate cerium valence and short Ce–Ru bonds.

Together Ir and Si atoms build up a three-dimensional $[Ir_2Si_2]$ network in both modifications. The Ir–Si distances range from 2.41 to 2.44 Å, in good agreement with the sum of the covalent radii [34] of 2.44 Å, indicating substantial Ir–Si bonding. This is addressed in more detail in the chemical bonding section (*vide infra*). While no direct Si–Si contacts are observed in β-$CeIr_2Si_2$, Si_2 pairs with 2.52 Å Si–Si distance occur in α-$CeIr_2Si_2$. These distances are much longer than in the diamond modification of silicon (2.35 Å) [35].

Although the shortest Ce–Ce distances in both modifications (4.09 Å in α-$CeIr_2Si_2$ and 4.15 Å in β-$CeIr_2Si_2$) are well above the Hill limit for *f* electron localization [36], one observes non-integer cerium valence. For further crystal chemical details on α- and β-$CeIr_2Si_2$ we refer to the original crystallographic work [13]. In the following sections we focus on the electronic structure and chemical bonding in this fascinating silicide.

3. Computational details

Within DFT we use two complementary computational methods. The Vienna *ab initio* simulation package (VASP) code [37,38] allows geometry optimization and subsequent establishment of the energy–volume equations of states for the α and β forms of $CeIr_2Si_2$. For this we use the projector augmented wave (PAW) method [39] (particularly accurate for studying rare earths), built within the generalized gradient approximation (GGA) scheme following Perdew, Burke and Ernzerhof (PBE) [40]. The conjugate-gradient algorithm [41] is used in this computational scheme to relax the atoms of the different crystal setups. The tetrahedron method with Blöchl corrections [39] as well as a Methfessel–Paxton [42] scheme were applied for both geometry relaxation and total energy calculations. Brillouin-zone (BZ) integrals were approximated using the special *k*-point sampling of Monkhorst and Pack [43]. The optimization of the structural parameters was performed until the forces on the atoms were less than 0.02 eV/Å and all stress components less than 0.003 eV/Å^3. The calculations are converged at an energy cut-off of 273 eV for the plane-wave basis set with respect to the *k*-point integration with a starting mesh of $4\times4\times4$ up to $8\times8\times8$ for best convergence and relaxation to zero strains. Then all-electron calculations, equally based on the DFT with GGA-PBE functional [40], are carried out for a full description of the electronic structure and the properties of chemical bonding. They are performed using the full potential scalar-relativistic augmented spherical wave (ASW) method [44]. In the ASW method, the wave function is expanded in atom-centered augmented spherical waves, which are Hankel functions and numerical solutions of Schrödinger's equation, respectively, outside and inside the so-called augmentation spheres. In the minimal ASW basis set, we chose the outermost shells to represent the valence states and the matrix elements were constructed using partial waves up to $l_{max}+1=4$ for Ce, i.e., 4*f* states were considered within the basis set, $l_{max}+1=3$ for Ir and $l_{max}+1=2$ for Si. Self-consistency was achieved when charge transfers and energy changes between two successive cycles were such as: $\Delta Q<10^{-8}$ and $\Delta E<10^{-6}$ eV, respectively. The Brillouin zone integrations were performed using the linear tetrahedron method within the irreducible wedge [39]. The calculations were carried out assuming spin degenerate configuration. Besides the site projected density of states, we discuss qualitatively the pair interactions based on the overlap population analysis with the crystal orbital overlap population (COOP) [45]. In the plots, positive, negative, and zero COOP magnitudes indicate bonding, anti-bonding, and non-bonding interactions, respectively. Here we use the integrated *i*COOP criterion to address relative bonding intensities. We note that another scheme for describing the chemical bonding, the ECOV (covalent bond energy) criterion based on both the overlap and the Hamiltonian populations is also accessible within the ASW method [44]. It provides similar qualitative results to the COOP but tends to exaggerate the intensity of the ECOV involving *f* states.

4. Geometry optimization and energy–volume equations of state

Starting from the lattice parameters and the atomic positions determined from single crystal X-ray data for α- and β-$CeIr_2Si_2$ [13], we carried out a full geometry optimization. The optimized lattice parameters given in Tables 1 and 2 show a good agreement with the experimental data, especially for the internal atomic coordinates. Nevertheless despite the close magnitudes to experiment for the unit cell volumes, they differ in the trends, i.e. a slightly larger unit cell volume for the β phase versus the α phase. Also the calculated volumes are slightly larger than the experimental values due to the underbinding character of the GGA functional used to account for the exchange-correlation effects within DFT. But preliminary calculations with the local density approximation (LDA) functional [46] led to largely underestimated unit cell parameters. The other feature exhibited by the calculations is the stabilization of the β phase with respect to α. This is opposed to the energy trends observed with similar calculations for dimorphic YIr_2Si_2 [23] and $LaIr_2Si_2$ [24] where the α form is found to be more stable than the β form. In as far as the only difference is in the nature of Y and La which are trivalent in both forms while there is a trend to a change of the cerium valence to tetravalent in the β form, it becomes relevant to compare the relative energies with a tetravalent element homolog such as $ThIr_2Si_2$ [11,47]. For confronting the relative stabilities of the α/β phases at different volumes, the energy–volume equations of states (EOS) are calculated for all three compounds. In fact the calculated total energy pertains to the cohesive energy within the crystal because the solution of the Kohn–Sham DFT equations provides the energy with respect to infinitely separated electrons and nuclei. In as far as the zero of energy depends on the choice of the potentials, somehow it becomes arbitrary; i.e. it is shifted but not scaled. However, the energy derivatives as well as the EOS remain unaltered. For this reason one needs to establish the EOS and extract the fit parameters for an assessment of the equilibrium values. This is done from a (*E*,*V*) set of calculations around minima found from geometry optimization. The resulting

Table 1
Basic crystallographic data of body-centered tetragonal α-$CeIr_2Si_2$ ($ThCr_2Si_2$-type): Ce 2*a* (0,0,0); Ir 4*d* (0, 1/2,1/4).

α-$CeIr_2Si_2$, *I*4/*mmm* no. 139	Calc.	Exp. [13]
a (Å)	4.093	4.088
c (Å)	10.11	10.169
Unit cell volume (Å^3)	169.3	170.0
Energy (eV)	−79.301	
Si 4*e* (0,0,*z*)		
z_{Si}	0.379	0.3758
Shortest distances (Å)		
Ir–Si	2.43	2.411
Ce–Ir	3.25	3.262
Ce–Si	3.14	3.155

Table 2
Basic crystallographic data of tetragonal primitive β-$CeIr_2Si_2$ ($CaBe_2Ge_2$-type): Ir1 2*b* (1/4,3/4,1/2); Sil 2*a* (3/4,1/4,0).

β-$CeIr_2Si_2$, *P*4/*nmm* no. 129 Origin 2.	Calc.	Exp. [13]
a (Å)	4.150	4.146
c (Å)	9.931	9.855
Unit cell volume (Å^3)	171.5	169.4
Energy (eV)	−79.42	
Atoms at 2*c* (1/4,1/4,*z*)		
z_{Ce}	0.244	0.2448
z_{Ir2}	0.873	0.8735
z_{Si2}	0.630	0.6301
Shortest distances (Å)		
Ir2–Si2	2.41	2.399
Ir1–Si2	2.45	2.438
Ce–Ir1	3.28	3.260
Ce–Si1	3.16	3.180

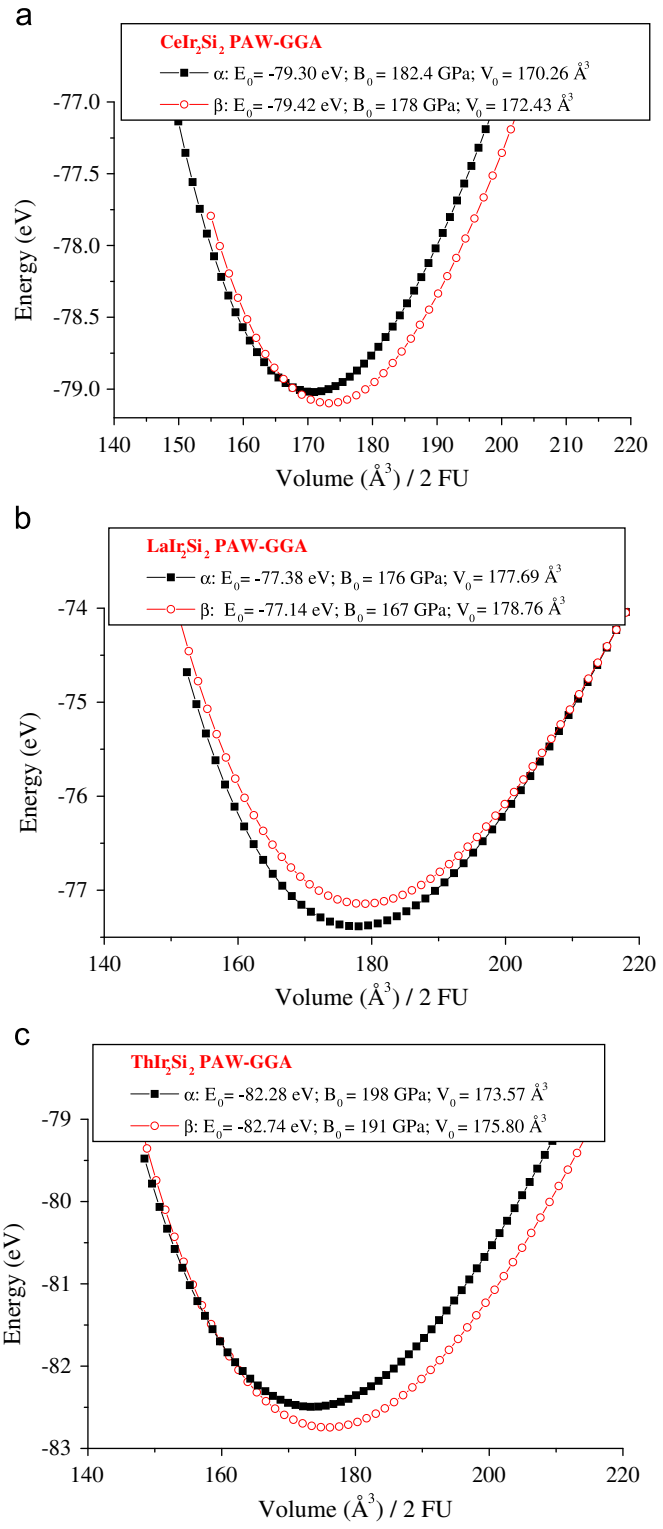

Fig. 2. Energy–volume curves for α- and β-forms of (a) $CeIr_2Si_2$, (b) $LaIr_2Si_2$ and (c) $ThIr_2Si_2$. Insets show fit values from Birch third order equation of state (see text).

$E=f(V)$ curves are shown in Fig. 2. They have a quadratic variation which can be fitted with an energy–volume Birch EOS to the 3rd order [48]:

$$E(V) = E_o(V_o) + [9/8]V_oB_o[([(V_o)/V])^{[2/3]} - 1]^2 + [9/16]B_o(B' - 4)V_o[([(V_o)/V])^{[2/3]} - 1]^3,$$

where E_o, V_o, B_o, and B' are the equilibrium energy, the volume, the bulk modulus, and its pressure derivative, respectively. For $CeIr_2Si_2$ the fit results in the inset of Fig. 2a show the above obtained geometry optimization trend of smaller volume of α versus β and the larger stability of the latter. Interestingly, the two curves tend to cross at volumes below equilibrium and the α form becomes more stable at small volumes.

The calculated $E(V)$ EOS for $LaIr_2Si_2$ and $ThIr_2Si_2$ were obtained with the same calculation procedure as for the $CeIr_2Si_2$ modifications. They are shown in Fig. 2(b) and (c). The stabilization of the α form versus β for $LaIr_2Si_2$ is in agreement with the literature but an opposite result is obtained for $ThIr_2Si_2$ with a stabilization of the β variety, just like $CeIr_2Si_2$. This agrees with the synthesis of this intermetallic only in this form [11,47]. In as far as Th is only stable in a tetravalent state, this gives support to the stabilization trend of Ce toward this valence state in $CeIr_2Si_2$, both experimentally and theoretically.

Furthermore, Mihalik et al. [20] showed that the β→α transition in $CeIr_2Si_2$ occurs at a lower temperature than those observed for the other rare earths. The calculated energy difference between α and β $CeIr_2Si_2$, $\Delta E = -0.12$ eV (Fig. 2), is the smallest with respect to the other computed silicides, $LaIr_2Si_2$ ($\Delta E = -0.24$ eV) and $ThIr_2Si_2$ ($\Delta E = -0.46$ eV). This result lets suggest that the α and β phases are close in stability in $CeIr_2Si_2$.

In all compounds the common trends are toward a larger volume for the β form with a subsequent lower bulk modulus B_0 whose magnitudes increase in the sequence La–Ce–Th along which the volumes decrease. However, the largest B_0 magnitude observed for $ThIr_2Si_2$ member follows from the already large value for the metal (B_0(Th) = 54 GPa) while those of La and Ce are smaller (~22 GPa). Lastly the pressure derivative B' is close to 4 for both phases, a value usually encountered [49].

The changes in the electronic structure and derived properties such as the chemical bonding are further discussed in the next section using all electrons calculations.

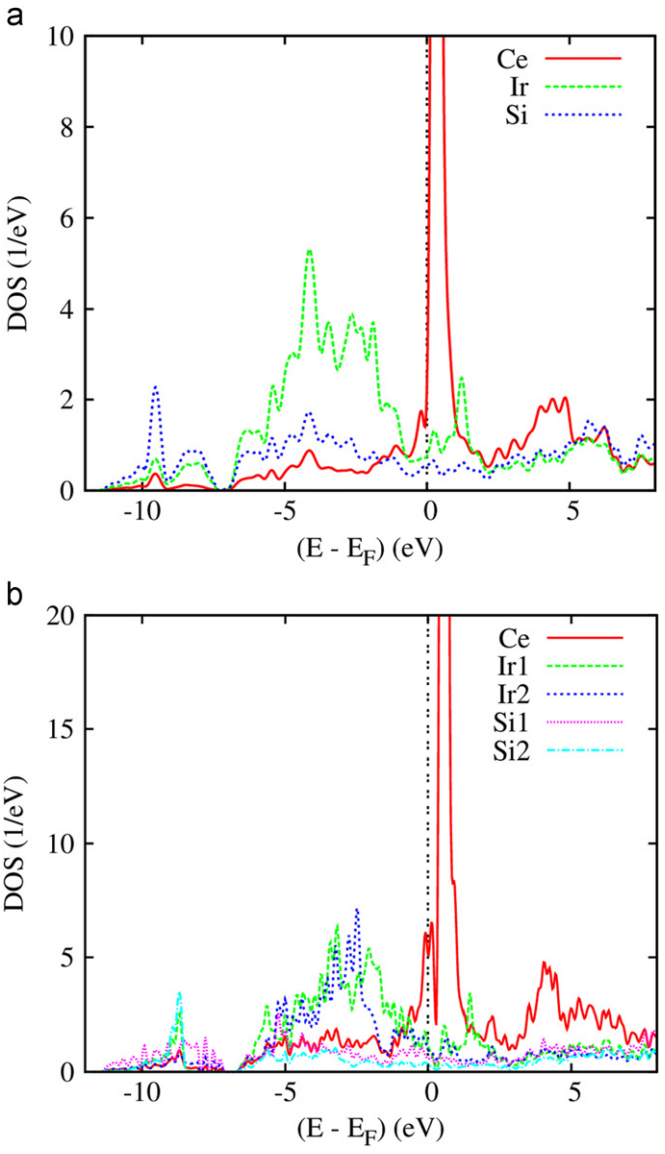

Fig. 3. $CeIr_2Si_2$: site projected density of states (DOS) for (a) α and (b) β forms.

5. All electrons calculations

5.1. Density of states

As far as the calculated crystallographic data in Table 1 are in relative agreement with experiment [13], we use the latter to examine the electronic band structure. At self-consistent energy convergence, little charge transfer was observed between the different species. There is, however, charge redistribution among the valence basis sets within the atomic species as well as between the different constituents leading to the bonding within the structure. This is detailed in Fig. 3 with the site projected density of states (PDOS) accounting for site multiplicities. In all panels the Fermi level (E_F) is at zero energy. This is also followed in COOP and *i*COOP plot below. We note here that the ASW calculations give the same energy trends of relative stabilities observed above, i.e. the larger stability of the β forms versus the α one, albeit with different magnitudes. Due to the difficult positioning of the (empty) 4*f* band (above E_F) in the framework of DFT, the DOS scale is restricted to small magnitude because the relevant information is in the occupied DOS (below E_F within the valence band (VB)), not in the virtual ones (above E_F within the conduction band (CB)).

The Fermi level crosses the lower part of Ce 4*f* with a low magnitude PDOS. This result agrees with the non-magnetically ordered state in the α and β modifications, i.e. the calculations in a spin-degenerate, non-spin-polarized configuration provide the ground state. The common features of the DOS are imposed by the atomic character of the constituents, i.e. rather empty Ce 4*f* ([Xe] $6s^2$ $5d^1$ $4f^1$) states are found above the Fermi level within the CB while largely filled Ir 5*d* ([Xe] $6s^2$ $5d^7$) are found below the Fermi level, within the VB. Interestingly the localization of Ce 4*f* resembled by the breadth of the 4*f* PDOS and their energy separations with respect to E_F are larger in the β phase as with respect to the α one. This agrees with the trend to the increase of the Ce valence from intermediate to tetravalent upon going from α to β as observed experimentally by Buffat et al. [12]. From the results the electronic contribution to the specific heat γ can be obtained:

γ (α-$CeIr_2Si_2$): 14.3 mJ/(mole K^2)

γ (β-$CeIr_2Si_2$): 25.2 mJ/(mole K^2)

The large increase of γ in the sequence α→β is concomitant with the increase of the Ce(*f*) PDOS at the Fermi level and it is

supported by experimental data on β and α cerium, the latter being tetravalent [50].

The quantum mixing of the valence basis sets leading to the chemical bonding is ensured by the itinerant states within the VB. This is signaled by the similar shapes of the PDOS of Ce, Ir and Si in the energy range {−7 eV, E_F} for *p* and *d* states as well as at lower energies {−10, −8 eV} involving non-directional Si(s) states.

5.2. Chemical bonding

For a good understanding of the chemical bonding, one needs to examine the stacking sequences in the α and β forms which are as follows using the labeling in Fig. 1 of the crystal structures:

…Ce|**[Ir_2Si_2]**|Ce|**[Ir_2Si_2]**|Ce… in α-$CeIr_2Si_2$

and

…Ce|[$Si1_2Ir2_2$]|Ce|**[$Ir1_2Si2_2$]**|Ce|[$Si1_2Ir2_2$] … in β-$CeIr_2Si_2$

Note that [$Ir1_2Si2_2$] in the β phase is the same as in the α form; they are shown in bold characters above. We call this layer "A" and layer [$Si1_2Ir2_2$], "B".

Besides substantial bonding within the [Ir_2Si_2] blocks, interlayer connections could be expected from the distances:

In α-$CeIr_2Si_2$: *d*(Si–Si)=2.52 Å;

in

β-$CeIr_2Si_2$: *d*(Ir2–Si2)=2.40 Å.

The chemical bonding is discussed based on the COOP criterion and the integrated COOP (unit less *i*COOP) corresponding to an integration of the COOP: the larger the area below the *i*COOP, the larger the bonding is. Both are presented for the α phase, but the discussion will be shown to be more significant from the *i*COOP which are solely plotted for the β phase.

Starting from α-$CeIr_2Si_2$, the plots are shown in Fig. 4 for the COOP (a) and the *i*COOP (b). The VB is bonding in its major part except for small anti-bonding negative COOP intensities appearing at E_F. The largest bonding is for Ir–Si while Ce–Ir and Ce–Si show smaller and almost equal intensities due to the close Ce–Ir and Ce–Si around 3.2–3.1 Å while the Ir–Si separation is ∼2.4 Å. The smallest intensity arises from the Si–Si bonding with silicon belonging to two successive layers at *d*(Si–Si)=2.52 Å (cf. Fig. 1), much larger than in

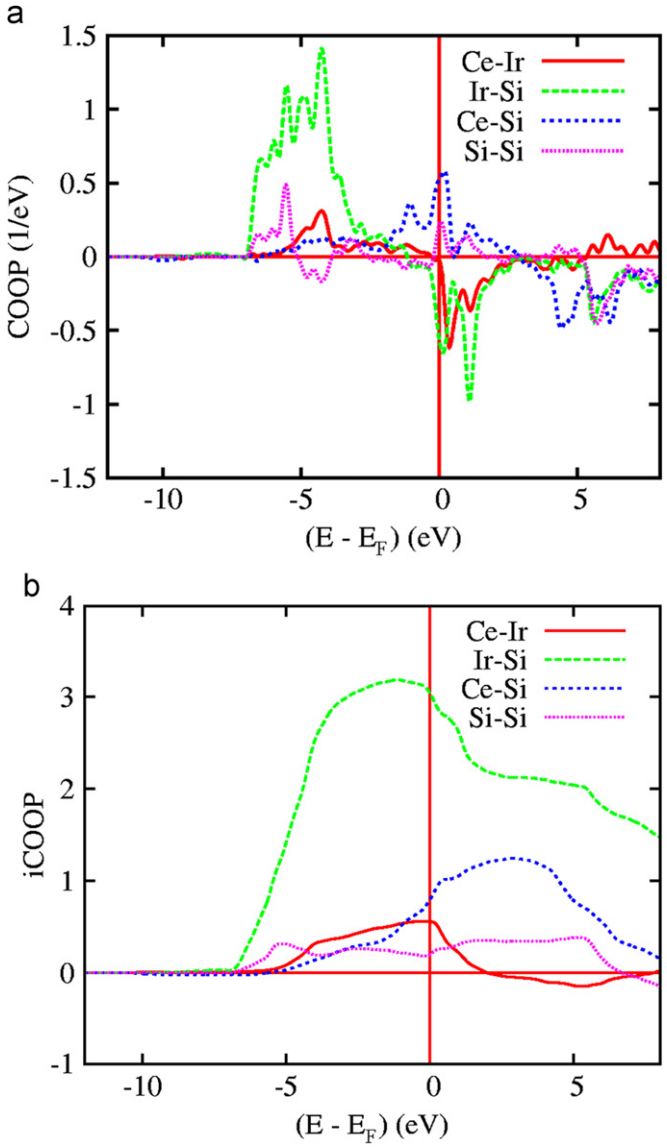

Fig. 4. α-$CeIr_2Si_2$: chemical bonding for pair interactions accounting for site multiplicities with (a) COOP and (b) integrated COOP (*i*COOP).

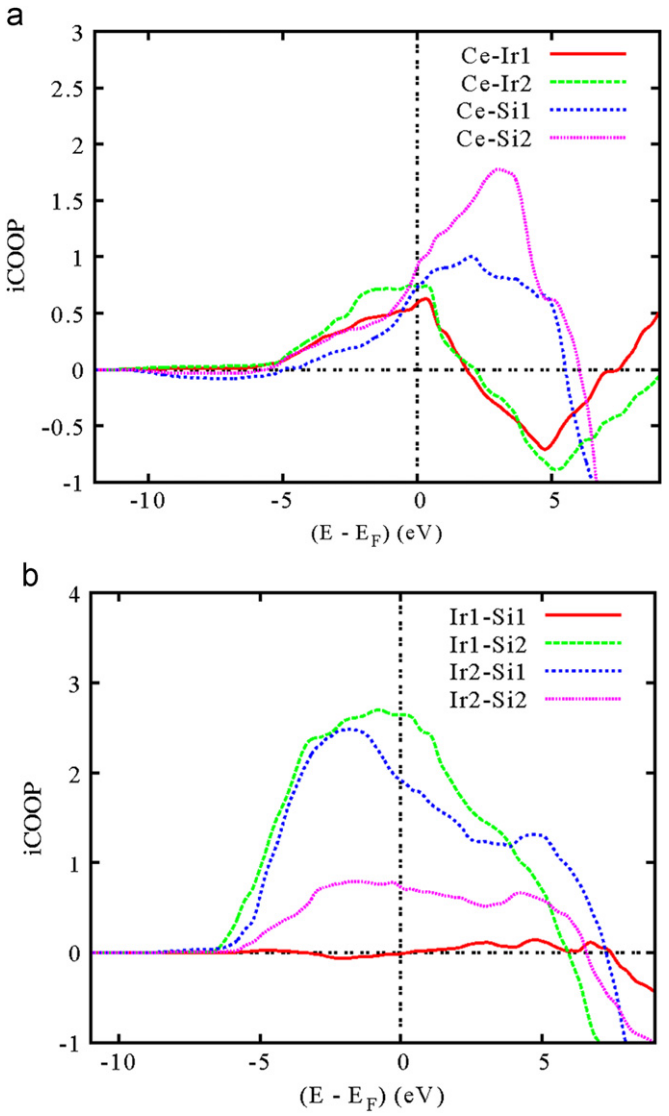

Fig. 5. β-$CeIr_2Si_2$: chemical bonding with *i*COOP criterion for pair interactions accounting for site multiplicities: (a) Ce–Ir and Ce–Si bonding; and (b) interactions within the [Ir_2Si_2] substructures.

the diamond modification of elemental silicon (2.35 Å) [33]. The *i*COOP curves in the lower panel (Fig. 4b) illustrate the COOP results further by showing the dominating Ir–Si and the nearly equal other two interactions; the Si–Si bonding is weakest. Therefore we show in the following the *i*COOP for the β form which contains five different atomic sites for the three chemical species involved, Ce, Ir and Si.

In Fig. 5 the *i*COOP data are shown for the two types of interactions in two panels: those involving Ce in Fig. 5a and those involving Ir and Si in Fig. 5b. In panel (a), four interactions are shown with intensities similar to those of Fig. 4. There is a larger Ce–Ir2 *i*COOP area with respect to the other ones is due to the smaller d(Ce–Ir2)∼3.15 Å versus d(Ce–Ir1)=3.26 Å and Ce–Ir1 bonding resembles the *i*COOP observed in Fig. 4. Other relevant features appear for the Ir–Si *i*COOPs in Fig. 5b. Expectedly the Ir1–Si1 *i*COOP has negligible intensity since Ir1 and Si1 belong to two different layers largely separated, namely A and B. The Ir1–Si2 (layer A) interaction is the same as in α and shows similar intensity (Fig. 4b). Lower intensity *i*COOPs are found for Ir2–Si1 (B layer). Then the two layers constituting the β-form are not equivalent in bonding. Lastly it is relevant to note the significant Ir2–Si2 bonding occurring between the A and B layers, due to the relatively small Ir2–Si2 separation of 2.4 Å. This bonding is far larger than the Si–Si interaction identified in the α form. This interlayer bonding could be one of the origins for the stabilization of the β form as observed from the calculations of both the EOS and the all electron calculations, but also the Ce^{IV}–Ir interactions.

6. Conclusion

The rarely observed phenomenon of valence driven structural dimorphism has been examined for $CeIr_2Si_2$ with complementary computational tools with the well established framework of DFT, casting a new insight over this interesting compound. We have mainly shown that the unexpected (versus ternary *R* homologs such as YIr_2Si_2 and $LaIr_2Si_2$) stabilization of the high temperature, β form versus the α form, is in agreement with the trend to a tetravalent Ce. This was supported by confrontation with the energy–volume equations of states for the La, Ce as well as the Th members whereby $CeIr_2Si_2$ behavior: $E(\beta) < E(\alpha)$, resembles that of the compound containing a tetravalent actinide, Th.

Also the site projected density of states show different localization and energy separation versus E_F in the two forms, a result illustrated by a nearly twice larger electronic contribution to the specific heat γ for β-$CeIr_2Si_2$ in agreement with a tetravalent Ce and experimental results on elemental Ce. The chemical bonding analysis shows changes mainly on the [Ir_2Si_2] intralayer as well as interlayer interactions.

References

[1] K.R. Andress, E. Alberti, Z. Metallkd. 27 (1935) 126.
[2] G. Just, P. Paufler, J. Alloys Compd. 232 (1996) 1.
[3] P. Villars, K. Cenzual, Pearson's Crystal Data: Crystal Structure Database for Inorganic Compounds, Release 2009/10, ASM International®, Materials Park, OH, USA, 2010.
[4] A. Szytuła, J. Leciejewicz, Handbook of Crystal Structures and Magnetic Properties of Rare Earth Intermetallics, CRC Press, Boca Raton, USA, 1994.
[5] M. Rotter, M. Tegel, D. Johrendt, Phys. Rev. Lett. 101 (2008) 107006.
[6] M. Rotter, M. Pangerl, M. Tegel, D. Johrendt, Angew. Chem. 120 (2008) 8067.
[7] Z. Ban, M. Sikirica, Acta Crystallogr. 18 (1965) 594.
[8] B. Eisenmann, N. May, W. Müller, H. Schäfer, Z. Naturforsch. 27b (1972) 1155.
[9] E. Parthé, L. Gelato, B. Chabot, M. Penzo, K. Cenzual, R. Gladyshevskyy, TYPIX—Standardized Data and Crystal Chemical Characterization of Inorganic Structure Types. Gmelin Handbook of Inorganic and Organometallic Chemistry, 8th edition, Springer, Berlin, Germany, 1993.
[10] D. Kußmann, R. Pöttgen, U.Ch. Rodewald, C. Rosenhahn, B.D. Mosel, G. Kotzyba, B. Künnen, Z. Naturforsch. 54b (1999) 1155.
[11] X.Z. Wang, B. Lloret, N.G. Wee Lam, B. Chevalier, J. Etourneau, P. Hagenmuller, Rev. Chim. Miner. 22 (1985) 711;
E.H. El Ghadraoui, J.Y. Pivan, R. Guérin, O. Pena, J. Padiou, M. Sergent, Mater. Res. Bull. 23 (1988) 1345.
[12] B. Buffat, B. Chevalier, M.H. Tulier, B. Lloret, J. Etourneau, Solid State Commun. 59 (1986) 17.
[13] D. Niepmann, R. Pöttgen, Intermetallics 9 (2001) 313.
[14] K. Hiebl, C. Horvath, P. Rogl, J. Less-Common Met. 117 (1986) 375.
[15] J. Etourneau, B. Chevalier, J. Solid State Chem. 96 (1992) 211.
[16] R. Welter, K. Halich, B. Malaman, J. Alloys Compd. 353 (2003) 48.
[17] M.B. Tchoula Tchokonté, P. de, V. du Plessis, D. Kaczorowski, Physica B 404 (2009) 2992.
[18] M. Mihalik, M. Diviš, V. Sechovský, Physica B 404 (2009) 3191.
[19] M. Mihalik, Z. Matěj, M. Diviš, V. Sechovský, Intermetallics 17 (2009) 927.
[20] M. Mihalik, J. Pospíšil, A. Rudajevová, X. Marti, D. Wallacher, A. Hoser, T. Hofmann, M. Diviš, V. Sechovský, Intermetallics 19 (2011) 1622.
[21] C. Zheng, J. Am. Chem. Soc. 115 (1993) 1047.
[22] I.R. Shein, A.L. Ivanovskii, Phys. Rev. B 83 (2011) 104501.
[23] I.R. Shein, Physica B 406 (2011) 3525.
[24] H.F. Braun, T. Jarlborg, A. Junod, Physica B 135 (1985) 397.
[25] S.F. Matar, E. Gaudin, B. Chevalier, R. Pöttgen, Solid State Sci. 9 (2007) 274.
[26] B. Chevalier, E. Gaudin, A.F. Al Alam, S.F. Matar, F. Weill, B. Heying, R. Pöttgen, Z. Naturforsch. 63b (2008) 685.
[27] S.F. Matar, E. Gaudin, B. Chevalier, R. Pöttgen, Solid State Sci. 13 (2011) 948.
[28] S.F. Matar, A.F. Al Alam, M. Nakhl, R. Pöttgen, B. Chevalier, N. Ouaini, Solid State Sci. 13 (2011) 1704.
[29] K. Schäfer, W. Hermes, U.Ch. Rodewald, R.-D. Hoffmann, R. Pöttgen, Z. Naturforsch 66b (2011) 777.
[30] P. Hohenberg, W. Kohn, Phys. Rev. 136 (1964) B864.
[31] W. Kohn, L.J. Sham, Phys. Rev. 1140 (1965) A1133.
[32] W. Hermes, S.F. Matar, R. Pöttgen, Z. Naturforsch. 64b (2009) 901.
[33] T. Mishra, R.-D. Hoffmann, C. Schwickert, R. Pöttgen, Z. Naturforsch. 66b (2011) 771.
[34] J. Emsley, The Elements, Clarendon Press, Oxford, 1989.
[35] J. Donohue, The Structures of the Elements, Wiley, New York, 1974.
[36] H.H. Hill, Plutonium and Other Actinides, in: W.N. Mines (Ed.), Nuclear Materials Series 17, AIME, New York, 1970, p. 2.
[37] G. Kresse, J. Furthmüller, Phys. Rev. B 54 (1996) 11169.
[38] G. Kresse, J. Joubert, Phys. Rev. B 59 (1999) 1758.
[39] P.E. Blöchl, Phys. Rev. B 50 (1994) 17953.
[40] J. Perdew, K. Burke, M. Ernzerhof, Phys. Rev. Lett. 77 (1996) 3865.
[41] W.H. Press, B.P. Flannery, S.A. Teukolsky, W.T. Vetterling, Numerical Recipes, Cambridge University Press, New York, 1986.
[42] M. Methfessel, A.T. Paxton, Phys. Rev. B 40 (1989) 3616.
[43] H.J. Monkhorst, J.D. Pack, Phys. Rev. B 13 (1976) 5188.
[44] A.R. Williams, J. Kübler, C.D. Gelatt, Phys. Rev. B 19 (1979) 6094;
V. Eyert, The Augmented Spherical Wave Method—A Comprehensive Treatment, Lecture Notes in Physics, Springer, Heidelberg, 2007.
[45] R. Hoffmann, Angew. Chem. Int. Ed. Engl. 26 (1987) 846.
[46] S.H. Vosko, L. Wilk, M. Nusair, Can. J. Phys. 58 (1980) 1200.
[47] R.N. Shelton, H.F. Braun, E. Musick, Solid State Commun. 52 (1984) 797.
[48] F. Birch, J. Geophys. Res. 83 (1978) 1257.
[49] S.F. Matar, G. Demazeau, M.H. Möller, R. Pöttgen, Chem. Phys. Lett. 508 (2011) 21.
[50] O.V. Lounasmaa, Phys. Rev. B 133 (1964) A502.